Chapter 42
ONR MURI Project on Soil Blast Modeling and Simulation

Richard Regueiro, Ronald Pak, John McCartney, Stein Sture, Beichuan Yan, Zheng Duan, Jenna Svoboda, WoongJu Mun, Oleg Vasilyev, Nurlybek Kasimov, Eric Brown-Dymkoski, Curt Hansen, Shaofan Li, Bo Ren, Khalid Alshibli, Andrew Druckrey, Hongbing Lu, Huiyang Luo, Rebecca Brannon, Carlos Bonifasi-Lista, Asghar Yarahmadi, Emad Ghodrati, and James Colovos

Abstract Current computational modeling methods for simulating blast and ejecta in soils resulting from the detonation of buried explosives rely heavily on continuum approaches such as Arbitrary Lagrangian-Eulerian (ALE) and pure Eulerian shock-physics techniques. These methods approximate the soil as a Lagrangian solid continuum when deforming (but not flowing) or an Eulerian non-Newtonian fluid continuum when deforming and flowing at high strain rates. These two extremes do not properly account for the transition from solid to fluid-like behavior and vice versa in soil, nor properly address advection of internal state variables and fabric tensors in the Eulerian approaches. To address these deficiencies on the modeling side, we are developing a multiscale multiphase hybrid Lagrangian particle-continuum computational approach, in conjunction with coordinated laboratory experiments for parameter calibration and model validation. This paper provides an overview of the research approach and current progress for this Office of Naval Research (ONR) Multidisciplinary University Research Initiative (MURI) project.

Keywords Soil blast • Constitutive modeling • Multiscale computational modeling • Buried soil explosive geotechnical centrifuge experiments • X-ray computed tomography • Quasi-static to high strain rate experimental soil mechanics

42.1 Introduction

The problem of simulating the detonation, ensuing blast wave and ejecta from buried explosives in natural soils remains unsolved because of the wide variability (and uncertainty) in field conditions, ranging from soil type (cohesive versus cohesionless), density, moisture content (partially saturated versus saturated), height of water table, infiltration due to rainfall or snowmelt, presence of roots and/or thick grasses, etc. These conditions will vary depending on whether the explosive is an improvised explosive device (IED) buried in a roadside soil (Fig. 42.1), or a network of landmines placed across a beach. Worst case scenarios of field conditions could be tested and simulated for the combat theater of interest, and proper armoring technologies deployed on vehicles to withstand those conditions, tailoring the armoring for a specific theater.

R. Regueiro (✉) • R. Pak • J. McCartney • S. Sture • B. Yan • Z. Duan • J. Svoboda • W. Mun
Department of Civil, Environmental, and Architectural Engineering, University of Colorado, Boulder, 428 UCB, Boulder, CO 80309, USA
e-mail: richard.regueiro@colorado.edu

O. Vasilyev • N. Kasimov • E. Brown-Dymkoski • C. Hansen
Department of Mechanical Engineering, University of Colorado Boulder, 428 UCB, Boulder, CO 80309, USA

S. Li • B. Ren
Department of Civil and Environmental Engineering, University of California, Berkeley, 783 Davis Hall, Berkeley, CA 94720-1710, USA

K. Alshibli • A. Druckrey
Department of Civil and Environmental Engineering, University of Tennessee, 73A Perkins Hall, Knoxville, TN 37996-2010, USA

H. Lu • H. Luo
Department of Mechanical Engineering, University of Texas, Dallas, 800 West Campbell Rd, Mailstop: EC-38, Richardson, TX 75080-03021, USA

R. Brannon • C. Bonifasi-Lista • A. Yarahmadi • E. Ghodrati • J. Colovos
Department of Mechanical Engineering, University of Utah, 50 South Central Campus Drive, Rm 2202, Salt Lake City, UT 84112-9208, USA

B. Song et al. (eds.), *Dynamic Behavior of Materials, Volume 1: Proceedings of the 2013 Annual Conference on Experimental and Applied Mechanics*, Conference Proceedings of the Society for Experimental Mechanics Series,
DOI 10.1007/978-3-319-00771-7_42,

Fig. 42.1 Sequence of images from IED in Iraq hitting U.S. military convoy, demonstrating soil ejecta under asphalt pavement video.google.com

To address this problem, a research program is currently in place with the following main features: (i) integrated experimental mechanics and multiscale computational modeling; (ii) concurrent multiscale approach to simulating soil ejecta (i.e., open-window on pore-grain-scale representation of explosive region where ejecta forms, but with proper boundary conditions (BCs)); and (iii) hierarchical multiscale continuum constitutive modeling at high strain rates, pressures, and large deformations implemented in a multiphasic Lagrangian particle approach for shock wave and soil ejecta prediction. The overall research objective is to numerically predict (a) the propagation of blast waves in soil (accounting for physics at grain-to-application-blast length-and-time-scales); (b) explosive device fragment interaction with soil; and (c) the triphasic soil deformation, fracture, fragmentation and ejecta resulting from the detonation of a buried explosive device in various soil types (cohesive and cohesionless soils, dry to partially saturated and fully saturated) and in-situ material variations.

Soil is generally a triphasic porous medium, composed of a compressible solid (soil skeleton), liquid (usually water), and gas (usually air). For the solid and liquid constituents, a Lagrangian multiscale particle-continuum computational approach naturally provides the transition from solid-like to fluid-like material state upon blast loading, but keeping within a Lagrangian computational framework. The gas (i.e., air) constituent can most efficiently be modeled as a background Eulerian grid accounting for varying air temperature, pressure, humidity, etc., during blast wave propagation. The multiscale Lagrangian approach also more accurately resolves the interfacial mechanics between explosive fragments and soil ejecta resulting from the buried explosive device and ultimately impacting vehicles that need to be protected from such blasts. The main approach is to use a Lagrangian material particle description of the deforming/flowing biphasic (solid and liquid) soil around the initiation of buried explosion and fragmentation (Fig. 42.2), and around fragments as they eject through the soil along with the interacting soil masses. The finite element mesh would need to be adaptively converted to a 'particle' representation of the soil ahead of the blast wave and fragment path (Fig. 42.2), or a 'particle' representation is maintained in the path of the fragments and ejecta. In this particle region, sand grains are represented by discrete elements (DE) that can fracture under grain crushing, and cohesive soil clay matrix (providing cohesion between grains) is modeled using a meshfree 'particle' method with ability to fracture and fragment cohesive soil. The pore liquid can be incorporated directly into the variational meshfree particle formulation as a continuum mixture approximation, unless the soil is purely cohesionless (e.g., a sand) and modeled using DEs, whereby the pore liquid is modeled using another particle method like Smoothed Particle Hydrodynamics (SPH). The soil that behaves more solid-like outside the crater region will be modeled using a Lagrangian multiphase continuum constitutive model appropriate for large strains within a finite element framework, as a higher-order generalized continuum (triphasic micromorphic continuum) to properly account for large deformations and wave propagation (no artificial numerical wave reflections) at the transition from particle region to continuum FE region (Fig. 42.2). Farther away from the blast, the micromorphic continuum finite element model will transition to a viscoelastic dynamic boundary element method (BEM) formulation that allows the waves to propagate to

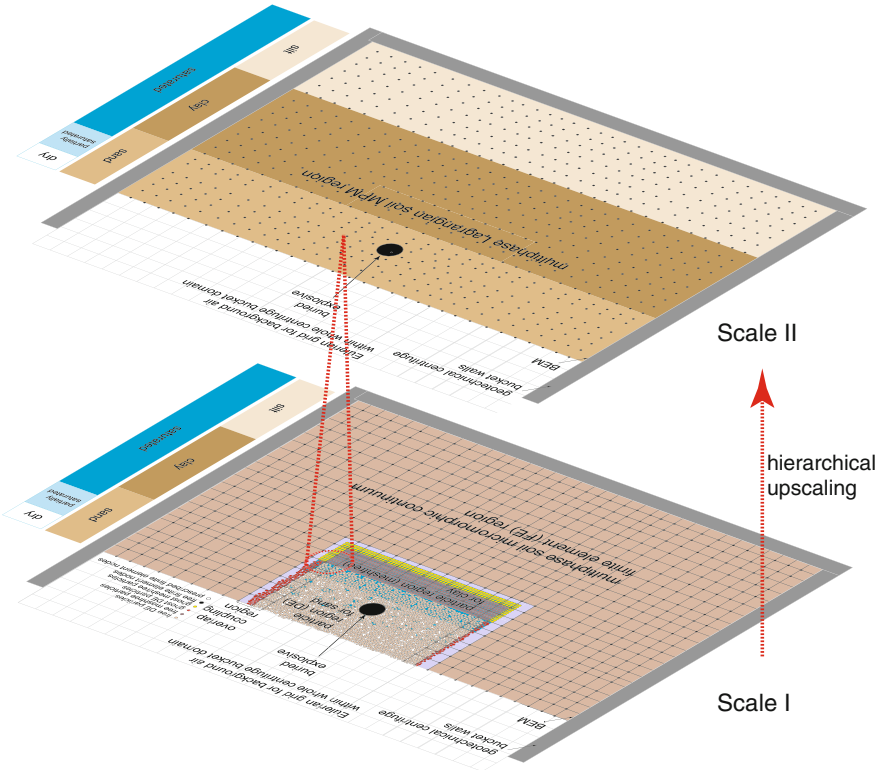

Fig. 42.2 2D illustrations (cross-sections through center of buried explosive) of 3D simulation setups for geotechnical centrifuge validation experiments (Fig. 42.7). Scale I: pore-grain-scale numerical modeling of soil with clay, silt/sand grains, and pore air and water. Scale II: hierarchical continuum constitutive model informed from Scale I; high-strain-rate, large deformation Uintah Material Point Method (MPM) implementation, and triphasic continuum formulation and implementation

infinity without wave reflection (or to represent boundary damping material used in the physical geotechnical centrifuge experiments) as well as other in-situ features such as layering and boulders.

To provide a physical validation of the hybrid coupled Discrete Element Method (DEM) – SPH – Reproducing Kernel Particle Method (RKPM) – Finite Element Method (FEM) – BEM – Computational Fluid Dynamics (CFD) multiscale modeling at Scale I and hierarchical continuum model at Scale II, scaled geotechnical centrifuge experiments (Fig. 42.7) are being conducted to obtain a high-fidelity, repeatable database on all key kinematic and kinetic aspects of the soil, water and air, including those of the ejecta, when subjected to buried explosive loading.

42.2 Technical Updates

42.2.1 High Strain Rate Split Hopkinson Pressure Bar (SHPB) Experiments on Boulder Clay and Mason Sand (Luo, Lu)

Dynamic compressive behavior of dry, partially saturated (as-received), and fully saturated Mason sand and Boulder clay under confinement was characterized using a long split Hopkinson pressure bar (SHPB). A sand sample is enclosed in a hardened steel tube with both ends capped by tungsten carbide rods which match the same mechanical impedance of the steel incident/transmission bars. This assembly is tapped to consolidate the sand grains to reach a desired mass density. For moist sand/clay, grease was used to fill the gap between the tungsten carbide rod and steel tube at each end to seal the ends to prevent the moisture to leak from the gap. For moist sand/clay, shaking assists water to distribute around the sand/clay grains. A moist specimen was kept for 2 days to allow even distribution of moisture. The actual moisture content was determined by weighing the assembly. A strain gage was attached on the external surface of the confining steel sleeve, to

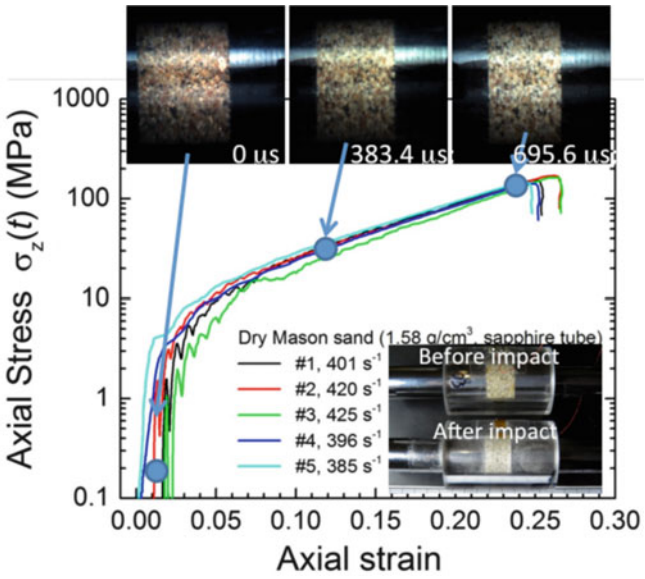

Fig. 42.3 Axial stress-axial strain curves of a dry Mason sand under confinement by a sapphire tube. Images acquired at frame rate 70 k fps show the sand deformation

measure the circumferential strain to allow calculation of the radial stress. This arrangement allows characterization of dynamic response to characterize the volumetric and deviatoric behavior. The void ratio as a function of pressure is determined at high strain rates. A copper disk was used as the pulse shaper. In this experiment, a striker bar of 2.13 m long was used. The incident bar was 8.74 m long, and the transmission bar was 8.74 m long. The stress-strain relationship under constrained impact, the specific energy absorption, and the compressibility of sand/clay were determined. To visually investigate the sand deformation, a transparent sapphire tube was used to confine the sand sample. A Cordin 550-62 high-speed camera was used to acquire the images (Fig. 42.3), which were analyzed using the digital image correlation (DIC) technique. The constitutive behavior is currently being analyzed by the University of Utah team to determine an appropriate constitutive model for these stress paths, and these data will also be used to calibrate the mesoscale computational modeling framework when it is capable of simulating in parallel computation so many sand grains, and clay matrix (when the Boulder clay and Mason sand are mixed in the future).

42.2.2 Quasi-static and Intermediate Strain Rate Triaxial Compression Experiments on Boulder Clay and Mason Sand (Svoboda, Mun, McCartney)

An important part of the project focuses on characterization of the properties of soils under high strain rates and high pressures that may be encountered during buried explosion events. The testing on rate effects focuses on the interpretation of results from axisymmetric triaxial compression tests on clay and sand specimens under saturated and unsaturated conditions with different rates of loading. Relevant results from these tests include the undrained shear strength, stiffness and pore water pressure generation. It is well established that faster loading rates lead to an increase in the undrained shear strength at a rate of approximately 10 % per log cycle of the time to failure. However, these studies did not thoroughly evaluate the influence of rate on shear-induced pore water pressure generation. Times to failure (defined as a failure strain of 20 %) range from 2 h for conventional loading rates to 0.1 s. Slow loading rates were applied in a typical triaxial compression test while faster loading rates were applied in a hydraulic press, both under displacement-controlled conditions. The results from this study indicate that substantial negative pore water pressures can be generated during rapid loading for sands, while positive pore water pressures can be generated for clays, as shown in Fig. 42.4. Unsaturated clays with suction values up to 100 kPa (degrees of saturation greater than 85 %) evaluated in constant water content tests have greater undrained shear strengths than saturated clays for a given loading rate, as expected, but the rate of increase in shear strength with loading rate is lower for unsaturated clays. This is attributed to the lower hydraulic conductivity of the unsaturated clay, as well as collapse of air voids during rapid loading. Overall, this study extends the body of knowledge on the influence of loading rates on clays under different initial conditions.

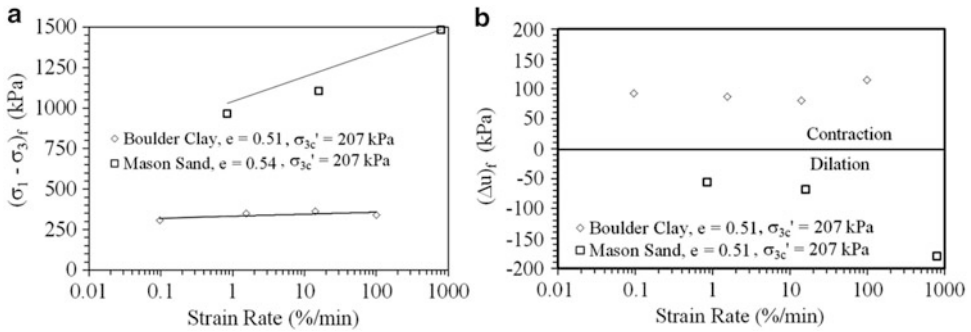

Fig. 42.4 Values at shear failure defined by the stress path tangency failure criterion: (**a**) Principal stress difference for Boulder clay and Mason sand; (**b**) Pore water pressure change for Boulder clay and Mason sand

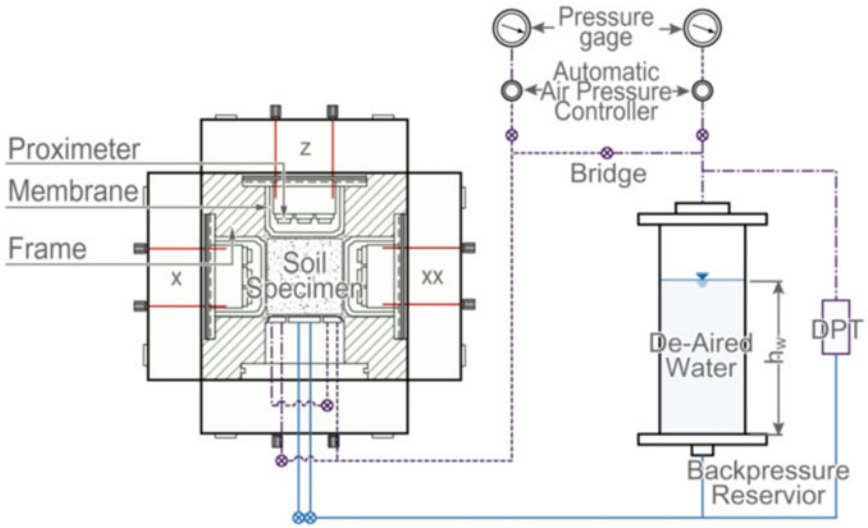

Fig. 42.5 Schematic of the pore-air/water pressure control/monitoring system for cubical cell

The investigation of high pressure effects in compression tests includes a series of tests to characterize the compression behavior of unsaturated compacted clay under higher stresses (up to 35 and 200 MPa). The role of suction on the preconsolidation stress and the slope of the compression curve are being investigated through a series of small diameter oedometer tests and larger-scale true-triaxial (cubical cell) tests on compacted specimens of the same clay under investigation in the rate effects study. A picture of the high pressure true triaxial cell with suction control is shown in Fig. 42.5. The behavior of unsaturated, compacted clay under net mean stresses up to 35 MPa in the oedometer and 200 MPa in the cubical cell have been investigated. These stress ranges are not only suitable for evaluation of the increase in the preconsolidation stress with increasing suction, but are also suitable for evaluation of the point at which the compression curves for different suction values converge and the compacted soil becomes a two-phase material. The curves for different suctions converge at the point where the air voids are compressed. Compression tests are being performed using both constant suction (drained air and water) and constant water content (undrained water, drained air) conditions. Different constitutive relationships for the compression behavior of unsaturated soils available in the literature are being investigated to represent these results, and will be correlated with the constitutive modeling at the University of Utah for this project.

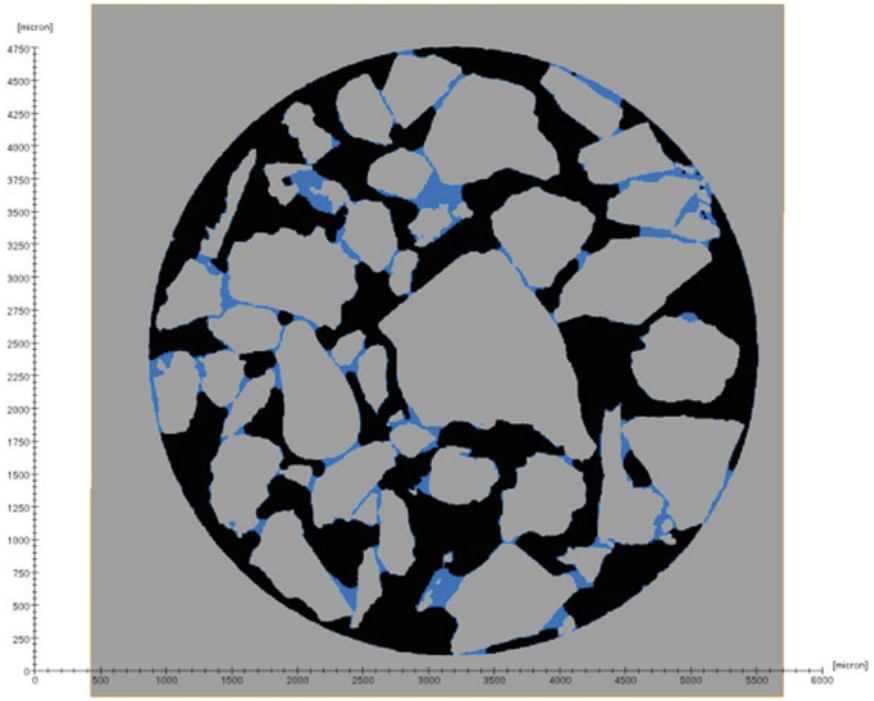

Fig. 42.6 Slice through a specimen of Mason sand showing water (*dark gray*), air (*black*), and particles (*gray*). Tube inner diameter = 4.5 mm

42.2.3 Synchrotron X-Ray Computed Tomography (CT) of Dry, Saturated, and Partially Saturated Mason Sand (Druckrey, Alshibli)

The research team at the University of Tennessee is conducting 3D characterization of the properties of Boulder clay and Mason sand soils at the micro-scale (grain-scale, for sand) using CT to measure the following properties: (1) Morphology of sand particles: samples of Mason sand were placed inside capillary tubes and were scanned using the CT technique for various moisture contents (Fig. 42.6). Particle shape and sphericity were quantified based on particle surface area, volume, longest, intermediate and shortest axes of particles. The geometry of air and water constituents in the voids are also quantified (Fig. 42.6). Such measurements can be used to generate DEM particles with interstitial air and water geometries. (2) Particle-to-particle interaction of sheared sand: in situ CT scans of a sand triaxial specimen were acquired for dry and partially saturated specimens to monitor particle interaction and particle-water interaction during shearing. The results of the analysis will be used to calibrate the mesoscale computational models for partially saturated condition. (3) Investigate the fabric of clay samples at meso-scale level: small samples of tested triaxial specimens will be scanned with the objective to quantify density variation within the sample. The CT technique will also be used to characterize the soil microstructure before and after the buried explosive soil geotechnical centrifuge experiments.

42.2.4 Geotechnical Centrifuge Experiments with Buried Soil Explosives (Hansen, Pak)

To provide a sound physical basis for an in-depth investigation of the buried soil blast problem, an experimental program using the geotechnical centrifuge modeling approach (e.g., Davies [1994], Pak and Guzina [1995], Pak and Soudkhah [2011]) is part of the project. The latest technology for capturing various kinematic and kinetic quantities involved in the high-rate soil dynamics problem, including high-g shock sensors, particle motion tracking, and high-speed cameras with three-dimensional digital image correlations are being tested and deployed in the experiments. Blasts of different intensity are being simulated using both explosive and non-explosive means. Some preliminary results for small-scale blasts using shock-tube type devices and explosives at normal gravity ("1g") in a soil model experiment are shown in Fig. 42.8, illustrating the appeal of both methods.

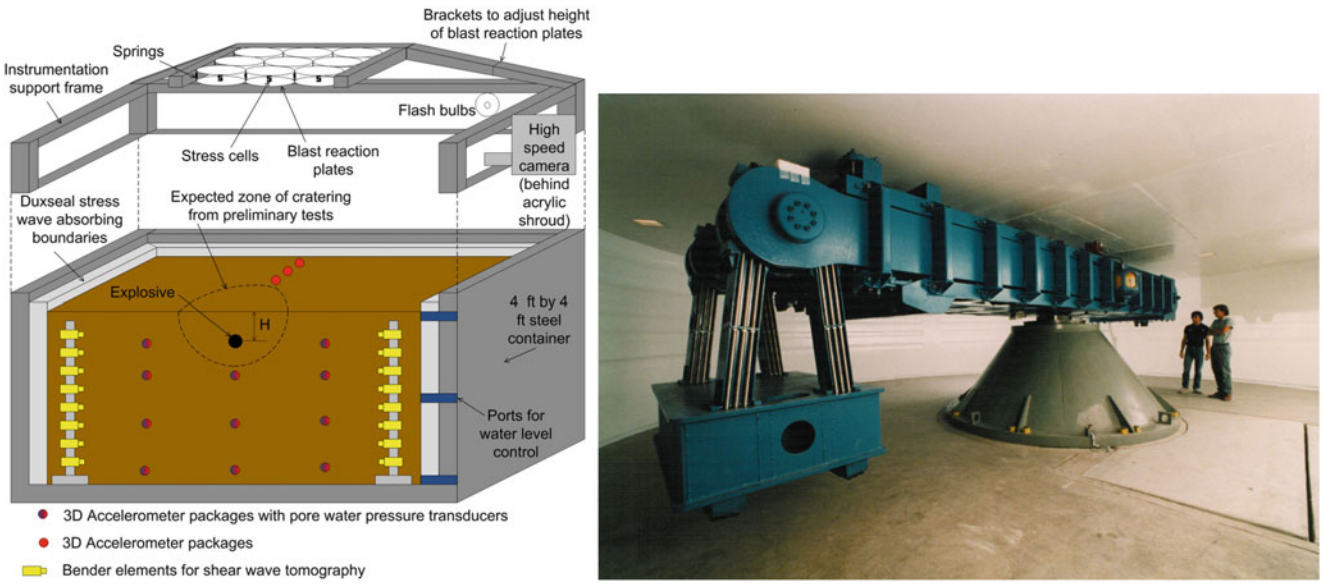

Fig. 42.7 (*Left*) Centrifuge testing setup and instrumentation plan. (*Right*) 400 g-ton geotechnical centrifuge at the University of Colorado Boulder

Fig. 42.8 (*Left*) Mason sand ejecta during shock-tube loaded experiment at 1g. (*Right*) Ejecta and crater formation during high explosive test in Mason sand at 1g

42.2.5 Constitutive Modeling and MPM Simulations for Buried Soil Blasts at Scale II (Bonifasi-Lista, Yarahmadi, Ghodrati, Colovos, Brannon)

The computational solid mechanics (CSM) group at the University of Utah is in charge of developing a high-strain-rate large-deformation continuum constitutive model for soils and implementing it in the material point method (MPM) with explosive loading in the Uintah open source software developed at the University of Utah (Scale II, Fig. 42.2). The MPM is a particle-grid method suitable for solving large deformations in which the constitutive model is history dependent and therefore intolerant to advection errors Sulsky et al. [1994]. The MPM has the advantages of both Eulerian and Lagrangian formulations. The soil constitutive model framework must support cohesive and cohesionless soils at various moisture contents. The macroscale model must be able to capture the influence of the microstructure (hierarchical upscaling between Scale I and Scale II, Fig. 42.2). It also has to be simple enough to be tractable in engineering simulations at large scales. Scaled geotechnical centrifuge tests are conducted to obtain kinematic and kinetic information of soil and subsequent ejecta when subject to buried explosive loading (Figs. 42.7, 42.8). Commonly used scaling laws are strain rate insensitive and hence require validation for soil blast simulations where high strain rate constitutive models are used. We present a simulation of blast loading in the geotechnical centrifuge experiment in Fig. 42.9. The goal of this work is to discern constitutive features essential for predicting results consistent with current scaling laws. A secondary goal is to assess the importance of Coriolis body forces in comparison to centrifugal forces. Preliminary studies of gas expansion in MPM using the recently developed Convected Particle Domain Interpolation (CPDI) integrator (Sadeghirad et al. [2011]) and integrators

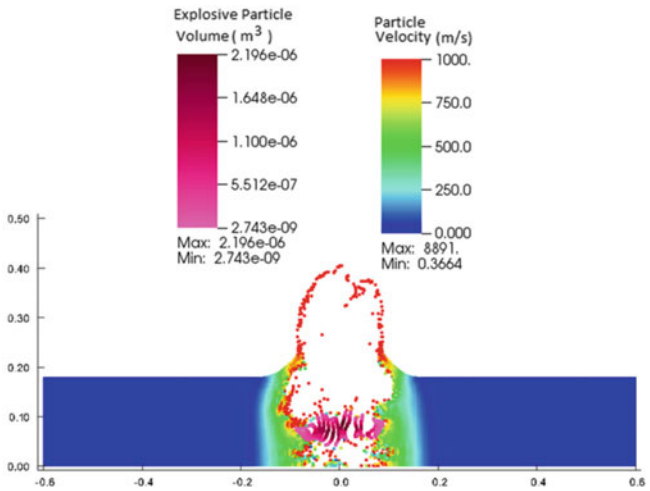

Fig. 42.9 Unlike the 1-g case, this 30-g centrifuge simulation produces two cavities (above and below the *pink-colored* explosive), and it has a visible asymmetry from Coriolis effects (color figure online)

based on the Generalized Interpolation Material Point (GIMP) method, show that the update of the deformation gradients are inconsistent with the update of the position of particles. Two sources of error are identified and analyzed. The first one involves the implementation of boundary tractions. Second, large and rapidly changing velocity gradients, common in blast simulations, appear to introduce numerical discrepancies in the kinematics updates. We will present a new method, called Multi-Point Query (MPQ) to ensure better consistency between updates of the deformation gradient and updates of particle locations.

42.2.6 RKPM/SPH Representation of Clay Fracture and Fragmentation at Scale I (Ren, Li)

A coupled RKPM (e.g., Danielson et al. [2000], Li and Liu [2004]) – SPH (e.g., Lu et al. [2005], Wang et al. [2005], and Bui et al. [2007]) formulation is being developed to simulate blast-induced clay matrix fracture and fragmentation at Scale I, and eventual coupling between clay matrix and sand grains at Scale I. The clay continuum is represented by RKPM zones, while the potential fracture planes are seeded by an SPH network. At the interface between RKPM and SPH, the SPH particles interact both with RKPM and SPH particles, thus bonding the RKPM clay continuum regions together. The SPH method updates the connectivities at every time step, allow the clay regions to separate into fragments. Using this RKPM-SPH coupling methodology for fracture and fragmentation of the clay matrix at Scale I, a cavity expansion simulation is conducted with result shown in Fig. 42.10.

42.2.7 Interaction of Soil Fragments and Background Air via Coupled Computational Fluid Dynamics (CFD) at Scale I (Brown-Dymkoski, Kasimov, Vasilyev)

In order to model flows around obstacles of complex geometries, such as compressible air or explosive gas around soil fragments, several approaches can are used. These methods can be separated into two major groups: body-fitted mesh and immersed boundary methods. The former uses conformal grids with nodes coincident to the surface of an obstacle, while the latter employs forcing upon the constitutive equations to impose appropriate boundary conditions. While body-fitted grids allow for exact boundary conditions to be imposed along the surface, grid meshing and re-meshing can be quite expensive and typically preclude the use of rectilinear grids. Moving and deforming obstacles are particularly problematic as they

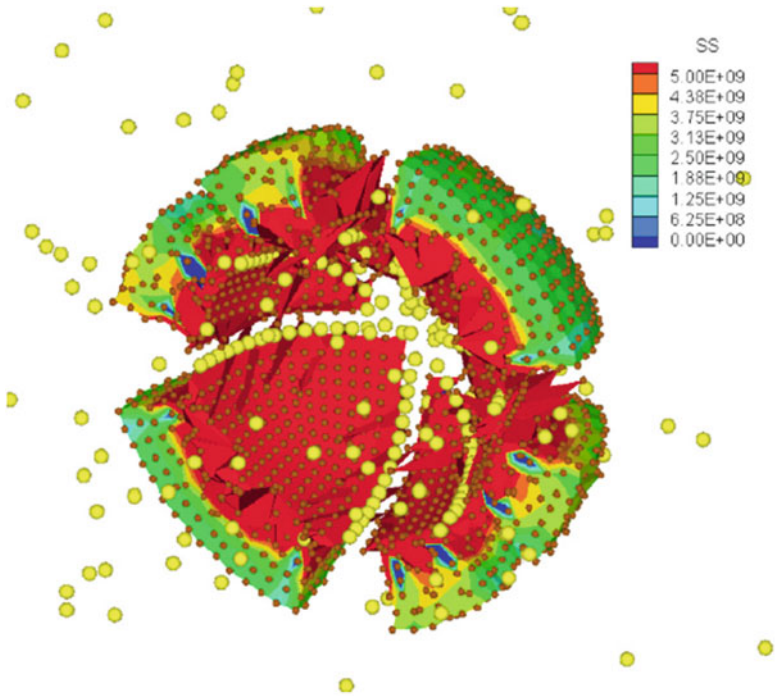

Fig. 42.10 Coupled RKPM-SPH blast simulation showing fracture and fragmentation along SPH layers. Contour values are von Mises stress

necessitate grid adaptation at every time step. Immersed boundary methods avoid the cost and complications of body meshing by introducing the effects of obstacles upon the governing equations themselves. Solid body effects, thus embedded within the flow itself, obviate the rigors of positioning nodes upon a surface. Immersed boundary forcing can be applied either to the continuous or discretized equations. While applying discretized forcing allows for a high level of control based upon the numerical accuracy and conservative properties of the discretization method, this approach lacks generality and flexibility across solvers (Mittal and Iaccarino [2005]). Volume penalization, on the other hand, imposes the effects of solid bodies by introducing forcing terms on the continuous equations and the resulting evolutionary equations are discretized and solved in the normal manner. One such method is the Brinkman Penalization Method (Angot et al. [1999]), which was originally developed for solid, isothermal obstacles in incompressible flows. A principal strength of Brinkman penalization is that error can be rigorously controlled a priori, with the solution converging to the exact in a predictable fashion (Feireisl et al. [2011], Kevlahan and Ghidaglia [2001]).

Brinkman Penalization Methods (Angot et al. [1999], Liu and Vasilyev [2007]), where solid obstacles are modeled as porous media with aporosity approaching zero, have been developed for incompressible andcompressible, viscous and inviscid flows. Until now, the main weakness of volume penalization approaches was the inability to model general boundary conditions, since they were limited to Dirichlet and homogeneous Neumann boundary conditions (Bae and Moon [2012], Kadoch et al. [2012]). This limitation precluded the use of Brinkman penalization for problems involving heat flux or shock reflection. In this work, a novel Characteristic-Based Volume Penalization (CBVP)approach is presented that builds upon Brinkman penalization but adds the flexibility of general boundary conditions. The premise of this new method is to use Brinkman-style forcing for Dirichlet type boundary conditions, while introducing linear convective terms to impose Neumann or Robin type conditions. Large coefficients on the penalization terms ensure that penalization acts on time scales much faster than the ones imposed by the physics. These penalization parameters allow for rigorous error control for each boundary condition type.

Characteristic-Based Volume Penalization (CBVP)

Application of boundary conditions is achieved by introducing additional terms within a penalized region representative of the solid obstacle. This CBVP method can be used to impose BCs for both integrated and non-integrated variables by appropriately combining the CBVP terms for each of the BCs. In this way, penalization can be easily formulated for a wide

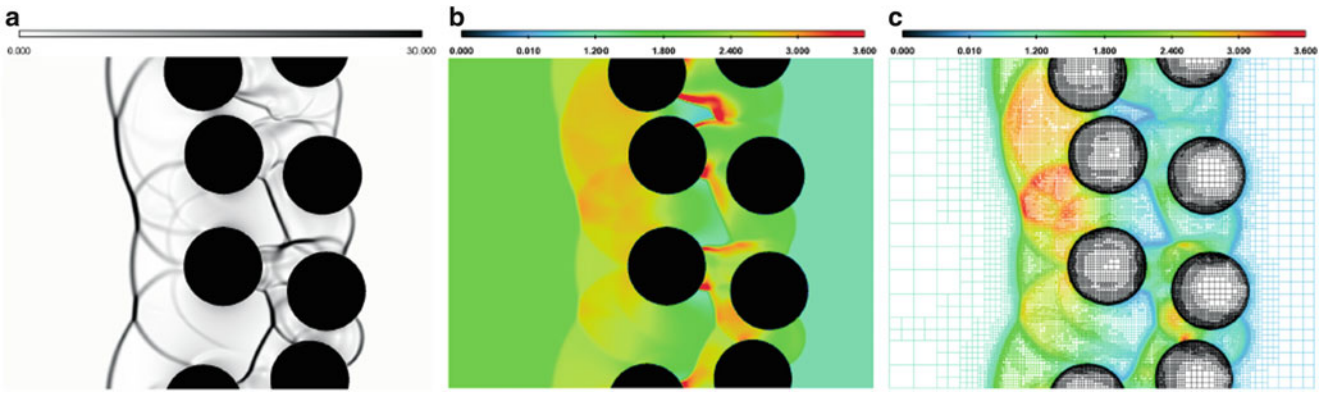

Fig. 42.11 Shock propagation through randomly packed cylinder array using CBVP method: (**a**) Schlieren image of the density field, (**b**) temperature field, and (**c**) computational mesh shaded by pressure field. Effective (non-adaptive) resolution is 1,153 × 896 grid points

variety of flow constitutive equations and BCs. Support of obstacle geometry for CBVP terms requires the definition of a spatial masking function to define the interior and exterior of an obstacle, as well as an additional definition of the normal within the obstacle. An example of a CBVP solution of the shock propagation through a randomly packed stationary cylinder array using Adaptive Wavelet Collocation Method (Vasilyev [2003]) is shown in Fig. 42.11. It should be noted that the CBVP method is applicable both for stationary or moving/deformable obstacles by appropriately modifying the forcing terms. This work is ongoing.

42.2.8 Hybrid OpenMP/MPI Parallel Code Framework for Discrete Element Method (DEM) at Scale I (Yan, Regueiro)

In support of the development of a new hybrid coupled DEM – SPH – RKPM – FEM – BEM – CFD multiscale modeling capability for soils at Scale I, a hybrid OpenMP/MPI parallel code framework is being developed, first for the DEM component of the multiscale model at Scale I. The parallelization starts from spatial domain decomposition and follows Foster's 4-step design methodology (partitioning, communication, agglomeration and mapping). A link-block algorithm is proposed for spatial partitioning and neighbor search (Fig. 42.12). The code is parallelized with message-passing interface (MPI) in distributed-memory mode, such that adjacent spatial blocks communicate through boundary cells; each block can in turn run in parallel with multiple threads in shared-memory (OpenMP) mode. It is expected that the hybrid parallel computing model adapts and scales well on Symmetrical Multiprocessing (SMP) clusters for maximum performance. We manage to minimize communication overhead, maintain adaptive spatial compute grids, keep load balance between compute nodes, handle particle migrations across computed nodes, and clear redundant contact information from adjacent processes, etc. Performance analysis of this parallel code such as speedup, efficiency, scalability is being evaluated based on computations carried out on SMP clusters (see Fig. 42.13).

42.2.9 Overlap Discrete Element (DE) and Micropolar Continuum Finite Element (FE) Coupling at Scale I (Duan, Regueiro)

The multiscale modeling at Scale I requires that we minimize the mesoscale modeling region around the explosive, ejecta, and cratering region in order to minimize computational effort. This requires applying proper BCs on the mesoscale modeling region, which entails overlap coupling of a micromorphic continuum FE implementation and the DE-SPH-RKPM-CFD mesoscale region as shown in more detail in Fig. 42.14 (left-top). We first start with a quasi-static overlap coupling problem between a 1D string of DE elastic particles and a 1D micropolar beam FE shown in Fig. 42.14 (Regueiro and Yan [2013]). Results are shown in Fig. 42.14, illustrating the complexity associated with the coupling between translational and rotational degrees of freedom for the DE model, that must be accommodated by the FE micropolar/micromorphic continuum model.

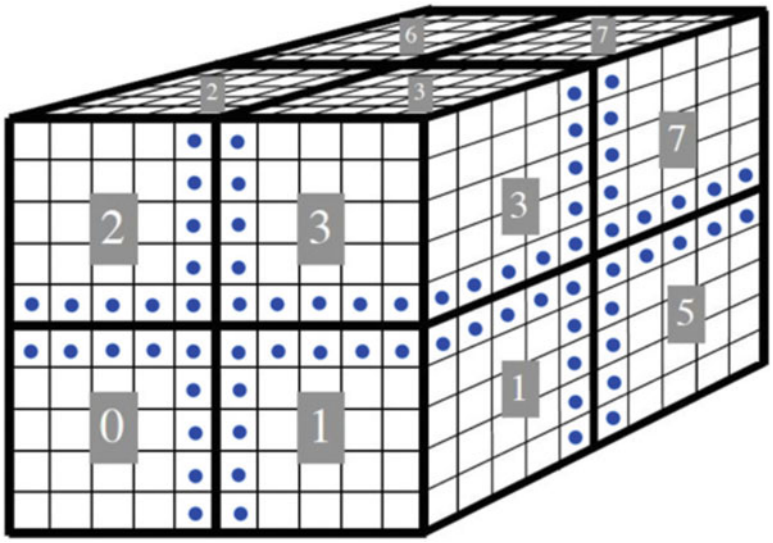

Fig. 42.12 The concept of link-block algorithm for DEM spatial partitioning and neighbor search

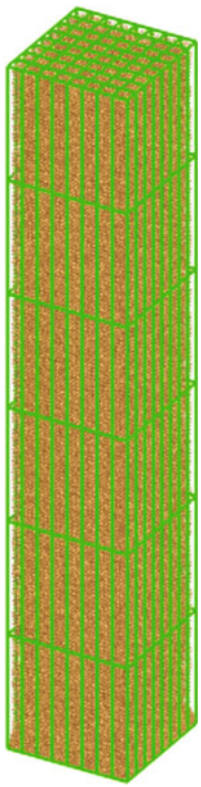

Fig. 42.13 $8 \times 8 \times 6 = 384$ grids for DE gravity deposition computation of 160,000 ellipsoidal particles

Most atomistic-continuum coupling methods ignore the rotational dofs, and thus the coupling is simpler to achieve for those methods. We are extending the overlap coupling to dynamics, micromorphic continuum FE, and eventually DE-SPH-RKPM-CFD for the mesoscale to which to overlap couple a triphasic micromorphic continuum FE.

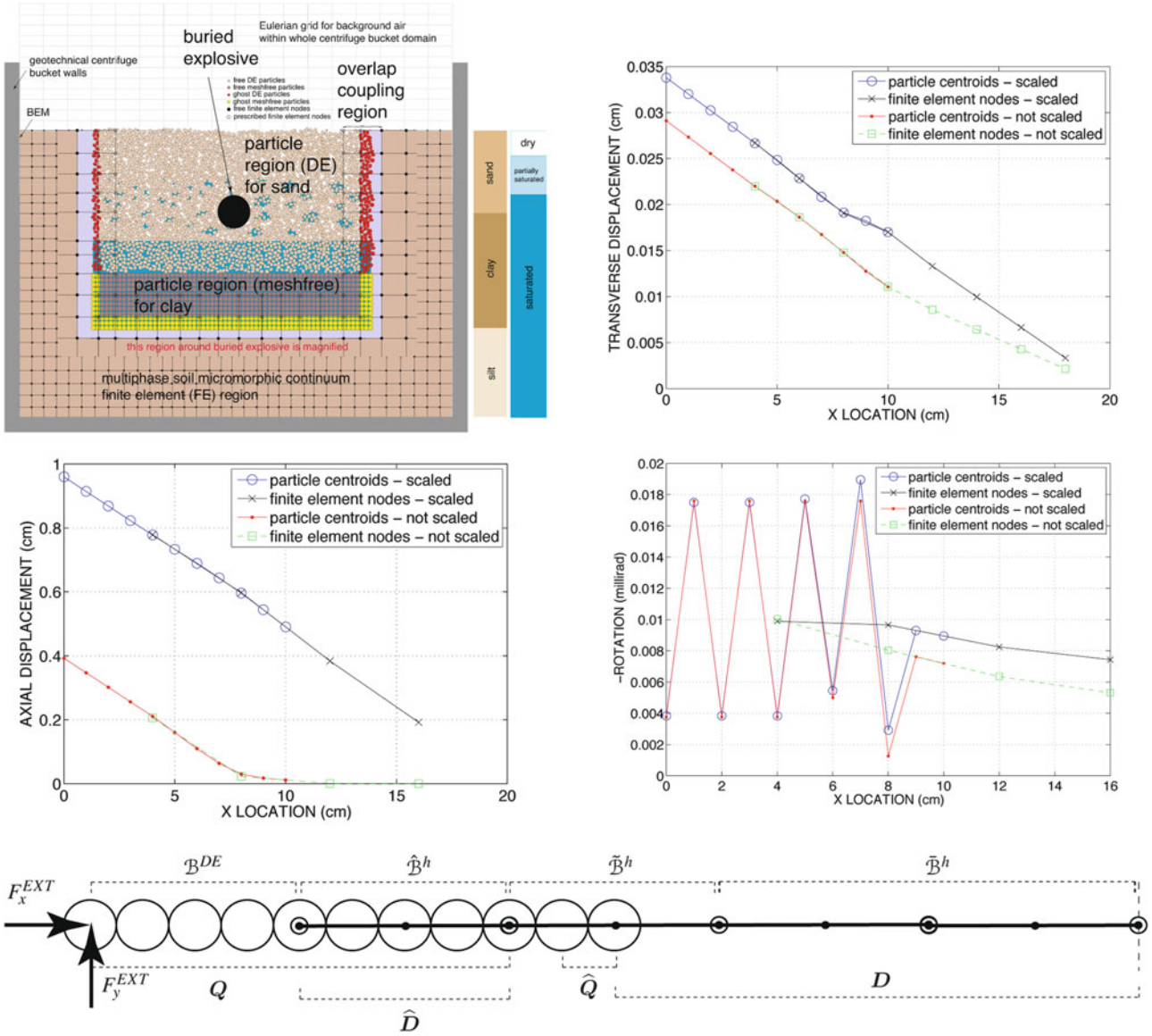

Fig. 42.14 (*Left-top*) Scale I (zoom in of explosive region): concurrent computational multiscale, multiphase failure mechanics of soil under buried explosive loading. (*Bottom*) Overlap coupling between 1D string of 11 DEs, and 4 micropolar FEs. (*Left-middle and right*) Axial displacement, transverse displacement, and rotational degrees of freedom showing scaled and not-scaled energy in the overlap region. The transverse displacement is coupled to the rotational dofs, thus there is a jog in the transition, as the rotational dofs from the DE and FE are significantly different (an artifact of the 1D DE string example, expected to reduce for 2D and 3D overlap coupling implementations)

42.3 Conclusion

We presented a brief overview and technical update of our ONR MURI project on soil blast modeling and simulation. Remaining work includes obtaining repeatable experimental data for homogeneous soils (Boulder clay and Mason sand), inhomogeneous soils (mix of Boulder clay and Mason sand), and layered soils in the geotechnical centrifuge buried explosive experiments, development and testing of Scale I coupled DE-SPH-RKPM-FEM-BEM-CFD code against small scale experimental results, hierarchical coupling between Scale I (mesoscale, or grain-scale, of soil) and Scale II (macroscale continuum modeling) and further modification of Scale II modeling based on upscaling and macroscale experimental data, Synchrotron X-ray CT characterization of mesoscale structure of soil in centrifuge tests (before and after explosive loading),

and combining all features of the project to simulate with some predictive capability the buried soil explosive geotechnical centrifuge experiments. Technology transfer to Department of Defense (DoD) researchers is already ongoing, and further interaction is welcome.

Acknowledgements Funding for this research was provided by Office of Naval Research (ONR) grant N00014-11-1-0691. This funding is gratefully acknowledged.

References

1. Angot P, Bruneau C-H, Fabrie P (1999) A penalization method to take into account obstacles in viscous flows. Numerische Mathematik 81:497–520
2. Bae Y, Moon YJ (2012) On the use of Brinkman penalization method for computation of acoustic scattering from complex boundaries. Comput Fluids 55:48–56
3. Bui HH, Fukagawa R, Sako K, Ohno S (2007) Lagrangian meshfree particles method (SPH) for large deformation and failure flows of geomaterial using elastic-plastic soil constitutive model. Int J Numer Anal Methods Géoméch 32(12):1537–1570
4. Danielson KT, Hao S, Liu W-K, Uras A, Li S (2000) Parallel computation of meshless methods for explicit dynamic analysis. Int J Numer Methods Eng 47:1323–1341
5. Davies MCR (1994) Dynamic soil-structure interaction resulting from blast loading. In: Leung et al (eds) Proceedings of the centrifuge 94, Balkema, pp 319–324
6. Feireisl E, Neustupa J, Stebel S (2011) Convergence of a Brinkman-type penalization for compressible fluid flows. J Differ Equ 250:596–606
7. Kadoch B, Kolomenskiy D, Angot P, Schneider K (2012) A volume penalization method for incompressible flows and scalar advection-diffusion with moving obstacles. J Comput Phys 231(12):4365–4383
8. Kevlahan NK-R, Ghidaglia J-M (2001) Computation of turbulent flow past an array of cylinders using a spectral method with Brinkman penalization. Eur J Mech B Fluids 20(3):333–350
9. Li S, Liu W-K (2004) Meshfree particle methods, 1st edn. Springer, Berlin
10. Liu Q, Vasilyev OV (2007) Brinkman penalization method for compressible flows in complex geometries. J Comput Phys 227(2):946–966
11. Lu Y, Wang ZQ, Chong K (2005) A comparative study of buried structure in soil subjected to blast load using 2D and 3D numerical simulations. Soil Dyn Earthq Eng 25(4):275–288
12. Mittal R, Iaccarino G (2005) Immersed boundary methods. Annu Rev Fluid Mech 37:239–261
13. Pak RYS, Guzina BB (1995) Dynamic characterization of vertically-loaded foundations on granular soils. J Geotech Eng 121(3):274–286
14. Pak RYS, Soudkhah M (2011) On experimental synthesis of seismic horizontal free-field motion of soil in finite-domain simulations with absorbing boundary. Soil Dyn Earthq Eng 31(11):1529–1539
15. Regueiro RA, Yan B (2013) Computational homogenization and partial overlap coupling between micropolar elastic continuum finite elements and elastic spherical discrete elements in one dimension. In: Li S, Gao X-L (eds) Handbook of micromechanics and nanomechanics, vol 1. Pan Stanford, Singapore, pp 1–45
16. Sadeghirad A, Brannon RM, Burghardt J (2011) A convected particle domain interpolation technique to extend applicability of the material point method for problems involving massive deformations. Int J Numer Methods Eng 86(12):1435–1456
17. Sulsky D, Chen A, Schreyer HL (1994) A particle method for history-dependent materials. Comput Methods Appl Mech Eng 118:179–196
18. Vasilyev OV (2003) Solving multi-dimensional evolotion problems with localized structures using second generation wavelets. Int J Comput Fluid Dyn (Special issue on High-resolut methods in Comput Fluid Dyn) 17(2):151–168
19. Wang ZQ, Lu Y, Hao H, Chong K (2005) A full coupled numerical analysis approach for buried structures subjected to subsurface blast. Comput Struct 83(4–5):339–356